ACS OMEGA

Article

Cite This: ACS Omega 2019, 4, 21975−21984

http://pubs.acs.org/journal/acsodf

NMR and Fluorescence Spectroscopies Reveal the Preorganized Binding Site in Family 14 Carbohydrate-Binding Module from Human Chitotriosidase

Eva Madland,[†] Oscar Crasson,[‡] Maryléne Vandevenne,[‡] Morten Sørlie,[§] and Finn L. Aachmann*[,†]

[†]Department of Biotechnology and Food Science, Norwegian Biopolymer Laboratory (NOBIPOL), NTNU Norwegian University of Science and Technology, Trondheim 7491, Norway

[‡]InBioS—Center for Protein Engineering, Institut de Chimie B6a, Université de Liège, Sart-Tilman, Liège 4000, Belgium

[§]Department of Chemistry, Biotechnology and Food Science, NMBU Norwegian University of Life Sciences, Ås 1430, Norway

Supporting Information

ABSTRACT: Carbohydrate-binding modules (CBM) play important roles in targeting and increasing the concentration of carbohydrate active enzymes on their substrates. Using NMR to get the solution structure of CBM14, we can gain insight into secondary structure elements and intramolecular interactions with our assigned nuclear overhauser effect peaks. This reveals that two conserved aromatic residues (Phe437 and Phe456) make up the hydrophobic core of the CBM. These residues are also responsible for connecting the two β-sheets together, by being part of β2 and β4, respectively, and together with disulfide bridges, they create CBM14's characteristic "hevein-like" fold. Most CBMs rely on aromatic residues for substrate binding; however, CBM14 contains just a single tryptophan (Trp465) that together with Asn466 enables substrate binding. Interestingly, an alanine mutation of a single residue (Leu454) located behind Trp465 renders the CBM incapable of binding. Fluorescence spectroscopy performed on this mutant reveals a significant blue shift, as well as a minor blue shift for its neighbor Val455. The reduction in steric hindrance causes the tryptophan to be buried into the hydrophobic core of the structure and therefore suggests a preorganized binding site for this CBM. Our results show that both Trp465 and Asn466 are affected when CBM14 interacts with both $(GlcNAc)_3$ and β-chitin, that the binding interactions are weak, and that CBM14 displays a slightly higher affinity toward β-chitin.

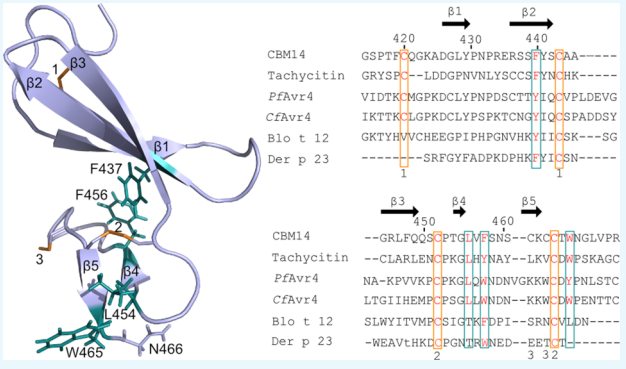

INTRODUCTION

Protein−carbohydrate interactions are involved in numerous biological processes, such as cell−cell recognition, fertilization, embryogenesis, and tumor metastasis among others.[1] Proteins involved in such interactions often have noncatalytic modules called carbohydrate-binding modules (CBMs). CBMs are subdivided into families according to their amino acid sequence similarity. They are currently classified into seven "fold families", which are further divided into three types. Type A binds to crystalline surfaces, B to glycan chains, and C to short oligosaccharides.[2] CBMs also show different ligand specificities, and there are characterized CBMs that interact with chitin, cellulose, starch, and other substrates.[3]

Chitin or β-1,4-linked *N*-acetylglucosamine (GlcNAc) is a linear and water-insoluble polymer that is an abundant component in the cell walls of fungi and the exoskeleton of crustaceans (i.e., crab, shrimp, and insects).[4] Chitin is not produced by mammals, making the polymer a likely candidate to trigger an innate immune response.[5] Lectins and other defense proteins are known to play an important role in initiating this immune response. Carbohydrate active enzymes contain many members, among them are chitinases that catalyze the hydrolysis of chitin. Chitinases are synthesized by both animals and plants that are not able to produce chitin, which underlines their importance in their immune defense and thus their ability to survive.[6]

In humans, two active chitinases have been reported: chitotriosidase-1 (CHIT1) and acidic mammalian chitinase. In addition, a chitobiase is synthesized that catalyzes the hydrolysis of a soluble GlcNAc dimer.[7,8] CHIT1 is synthesized as a 50 kDa soluble protein able to hydrolyze chitin.[9] This human chitinase is classified as belonging to family 18 of glycosyl hydrolases (GH18) in the Carbohydrate-Active-enZymes (CAZy) database (http://www.cazy.org).[10] It consists of two domains: a catalytic domain that adopts the conserved $(\alpha/\beta)_8$ TIM barrel form typical for GH18 and a noncatalytic domain in the N-terminal belonging to a CBM in family 14 (CBM14), which many of its members are known to

Received: September 17, 2019
Accepted: November 26, 2019
Published: December 9, 2019

DOI: 10.1021/acsomega.9b03043
ACS Omega 2019, 4, 21975−21984

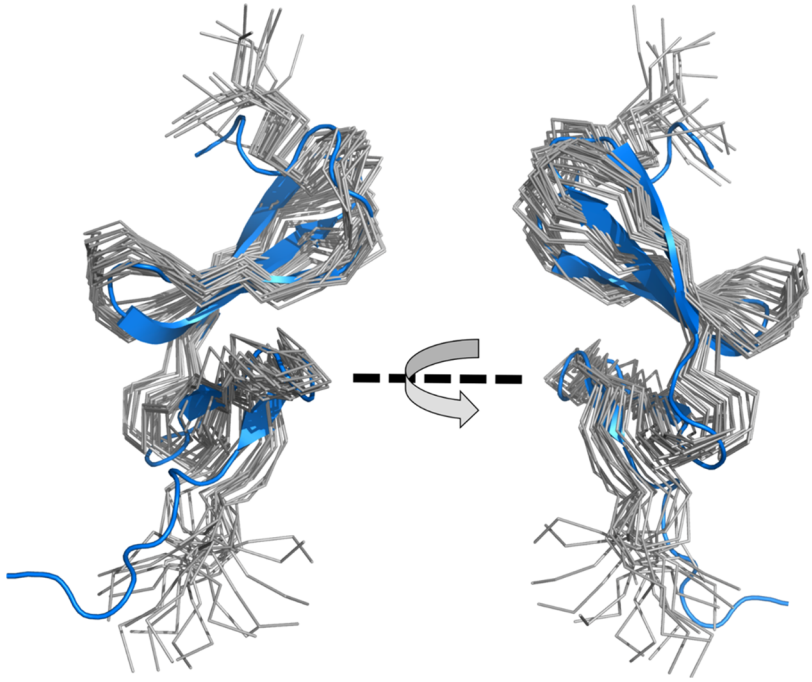

Figure 1. NMR solution structure of CBM14. Backbone representation of the 20 conformers with the lowest CYANA target function. The X-ray structure (PDB ID: 5HBF) is highlighted in blue. By aligning the X-ray structure with the 20 conformers determined by NMR spectra, the calculated RMSD is 1.59 Å over residues involved in β-sheets (Table S2).

bind chitin according to the CAZy database. These two domains are separated by a proline-rich and extended linker (PT-linker) that comprises 31 residues. The flexible nature of this linker could suggest that CBM14 works as a guiding system for CHIT1.[11] CBM family 14 has a lectin-like property of binding small sugars (mono-, di-, and trisaccharides) and is characterized by its highly conserved "hevein-like" fold.[3] The structure has three disulfide bonds that are important for its structural integrity as found by site-directed mutagenesis of either of the cysteins involved. It has also been shown that removal or mutagenesis of its only tryptophan has a detrimental effect on the CBMs ability to bind chitin.[12,13] Moreover, CHIT1 with its CBM degrades chitin faster and much more efficiently than its isoform without the CBM.[14]

According to CAZy, there are currently seven structures of CBM14s. Only two of the structures have been solved using NMR and correspond to tachycitin (PDB ID: 1DQC)[15] and dust mite allergen Blo t 12 (PDB ID: 2MFK). The remaining structures have been solved using X-ray crystallography, among which are CHIT1 (PDB ID: 5HBF) that includes the CBM14 elucidated by NMR here, Der p 23 (PDB ID: 4ZCE), a dust mite allergen from *Dermatophagoides pteronyssinus*,[16] and *Pf*Avr4 (PDB ID: 4Z4A), an effector protein from the tomato pathogen *Pseudocercospora fuligena*.[17] A structural homolog of *Pf*Avr4 and *Cf*Avr4, an effector protein from the tomato pathogen *Cladosporium fulvum*, has recently[18] been co-crystalized with a chitin hexaoligosaccharide $(GlcNAc)_6$ (PDB ID: 6BN0). This is the first co-crystal structure of a CBM14 with an oligosaccharide. *Cf*Avr4 has an extended binding surface that can accommodate longer polysaccharide chains and the interaction with the substrate is through aromatic residues and hydrogen bonds, which is more reminiscent of a type B CBM than the type C common for CBM14s.[3] This protein contains an extended loop that hydrogen-bonds with the oligosaccharide, as well as linking an additional N-terminal α-helix to the first β-sheet. It also contains two residues (Gln69 and Lys84) that through mutation studies are shown to have a great effect on the binding. These aspects are not conserved in other CBM14s and can therefore explain the observed difference in binding mode.

We have used NMR spectroscopy to determine the solution structure of CBM14 from CHIT1. As a result, we have developed further insight into the structural elements important in keeping CBM14s binding affinity for chitin. This CBM shows a binding affinity toward both $(GlcNAc)_3$ and β-chitin, and through our studies, we have found that the same residues (Trp465 and Asn466) are involved in binding both substrates. However, a single mutation of Leu454 to alanine renders the CBM unable to bind. Leu454 does not show a significant change in chemical shift perturbation when CBM14 (wild type, wt) interacts with either substrates. Interestingly, with fluorescence spectroscopy, we observe that Leu454Ala displays a significant blue shift, meaning that the position of Leu454 in the protein structure is significant for the correct orientation of Trp465 and therefore the protein's ability to bind substrates.

RESULTS

Solution Structure of CBM14. The solution structure of CBM14 (PDB ID: 6SO0) was determined by NMR spectroscopy. Assignment of the backbone and side-chain chemical shifts for CBM14 are essentially complete (N, ^{H}N, C^{α}, H^{α}, and C′ > 92%; H and C side chains > 76%) (Figure S1). The mature protein contains the following amino acids for purification purposes: three extra amino acids (Gly-Ser-Pro) at the N-terminus and five extra amino acids (Gly-Leu-Val-Pro-Arg) at the C-terminus. Gly-Ser in the N-terminus have not been assigned. Due to their location in a flexible-loop region, Cys460 and Cys462 are not observed because of line

DOI: 10.1021/acsomega.9b03043
ACS Omega 2019, 4, 21975−21984

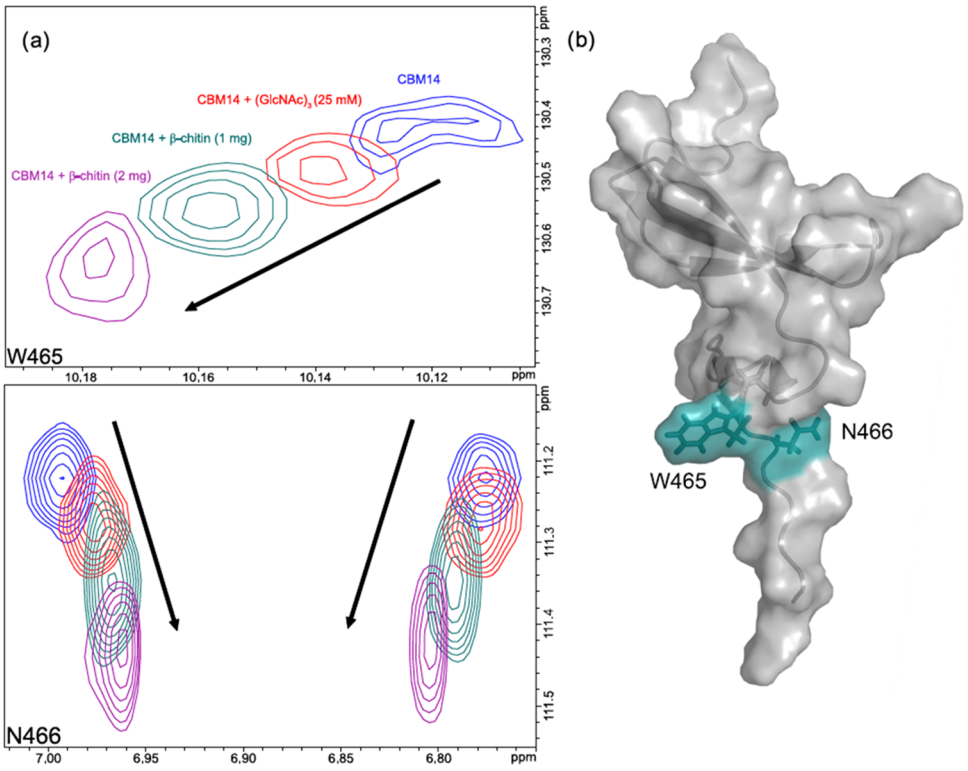

Figure 2. (a) ^{15}N-HSQC of the side chain of Trp465 and Asn466 of CBM14. The arrows indicate the direction in the change in chemical shift of CBM14 interacting with $(GlcNAc)_3$ (red) and β−chitin (turquoise and purple). This could suggest an increase in binding affinity for the crystalline substrate. (b) Surface representation of CBM14 showing Trp465 and Asn466 in blue.

broadening. Chemical shift data have been deposited at the Biological Magnetic Resonance Data Bank (BMRB) under the accession number 27277. The restraints and structural statistics for the 20 best conformers of CBM14 are given in Table S1.

The nuclear overhauser effect spectroscopy (NOESY) experiments show that the CBM14 fold comprises two β-sheets, three antiparallel β-strands in the N-terminal region (β1, β2, β3; residues 426−430, 436−442, and 444−449), and two antiparallel β-strands in the C-terminal region (β4, β5; residues 455−456 and 463−465). This fold pattern matches the previously described distorted β-sandwich fold in the crystal structure of the same protein,[11] and is known as the "hevein-fold". However, the two structures differ in the amount of amino acids involved in each β-strand (Table S2).

By aligning the NMR structure with the crystal structure (Figure 1), we obtain a root-mean-square deviation (RMSD) of 1.59 Å over the secondary structure (3.78 Å over 48 CA residues). The highest deviations are observed in the loop regions of the CBM.

Connecting β2 and β3 is a type I turn (residues 442−444). The protein contains six cysteins that form three disulfide bridges (Cys420-Cys440, Cys450-463, and Cys460-462) that have a stabilizing effect on the β-sandwich, also described by Fadel et al.[11] Through the NOESY experiments, we observed NOEs between two aromatic residues Phe437 and Phe456 involved in β2 and β4, respectively. These residues create a hydrophobic core holding the two β-sheets together. This core is probably essential for the β-sandwich fold given the conservation of aromatic residues in this position in other CBM14s.

Interaction with $(GlcNAc)_3$. The binding properties of CBM14 and $(GlcNAc)_3$ were investigated using isothermal titration calorimetry (ITC). The shape of the ITC binding curve is described by the so-called Wiseman c value,[19] which can be expressed as follows

$$c = nK_a[M]_t \quad (1)$$

where n is the stoichiometry of the reaction, K_a is the equilibrium binding association constant, and $[M]_t$ is the protein concentration. It is well established that c values within the range of $10 < c < 1000$ are a prerequisite for meaningful calculations of K_a.[19] A K_d of 9.9 mM (K_a = 100 M^{-1}) has previously been observed by Crasson et al.[13] With a protein concentration of 45 μM, typical for an ITC experiment, it is suggested that the c value would be close to 0.05. It has been shown that binding thermodynamics can be obtained even if c is in the range of $0.01 < c < 10$ if a sufficient portion of the binding isotherm is used for analysis.[20] This is achieved by ensuring a high molar ratio of ligand versus protein at the end of the titration, accurate knowledge of the concentrations of both ligand and receptor, an adequate level of signal-to-noise ratio in the data, and known stoichiometry. Using this approach, the fit of theoretical data to the experimental data (Figure S2) for four independent measurements yielded a K_d of 3.1 ± 0.2 mM and a ΔH_r° of −1.6 ± 0.2 kcal/mol. Moreover, a ΔG_r° of −3.3 ± 0.1 kcal/mol and a ΔS_r° of 6 ± 1 cal/kmol ($-T\Delta S_r^\circ$ = −1.7 ± 0.2 kcal/mol) can be calculated from eq 2. The obtained K_d is close to that previously observed.

$$\Delta G_r^\circ = \Delta H_r^\circ - T\Delta S_r^\circ = -RT \ln K_a = RT \ln K_d \quad (2)$$

Interaction Studies by NMR. To investigate whether binding of a different substrate, β-chitin, behaved in the same way as $(GlcNAc)_3$, we performed ^{15}N-heteronuclear single-

DOI: 10.1021/acsomega.9b03043
ACS Omega 2019, 4, 21975−21984

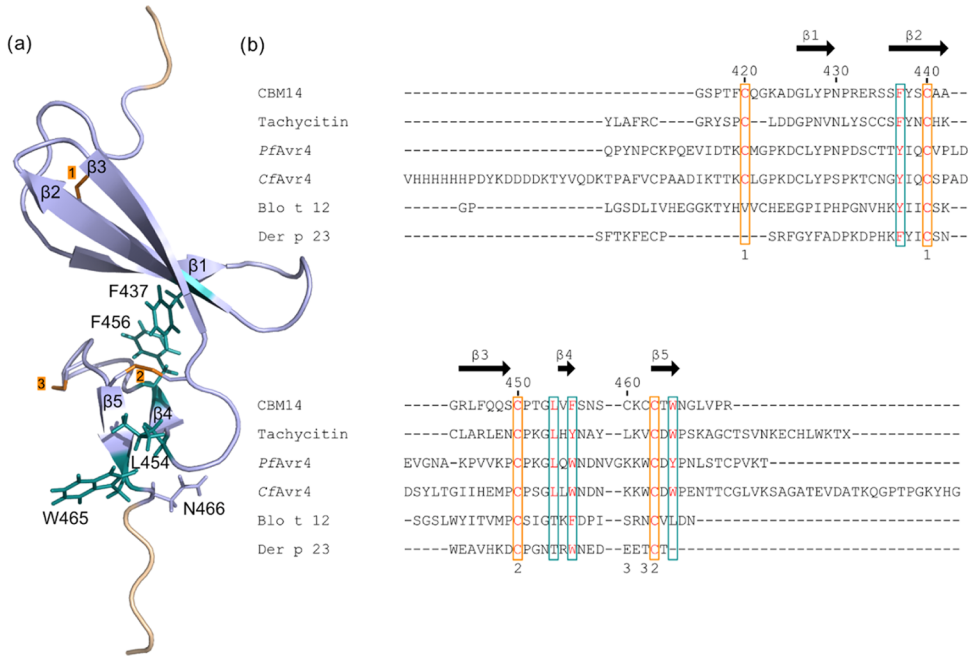

Figure 3. (a) One of the conformers of the NMR structure of CBM14 with labeled disulfide bridges (orange) and β-strands. The wheat color in both terminals corresponds to the residues added for purification purposes. Residues of particular interest includes their side chain and are highlighted in cyan (except for Asn466 which is added for its involvement in binding the substrate). (b) Multiple-sequence alignment performed using Clustal Omega (1.2.4) compares CBM14 from HCHT with five other CBM14s. Their sequence is collected from the Protein Data Bank (https://www.rcsb.org/). The conserved residues are highlighted in red, and orange boxes correspond to cysteins and cyan boxes to the residues in (a).

quantum correlation (HSQC) experiments on CBM14 alone and CBM14 together with β-chitin. This allowed us to investigate the chemical shift perturbation to probe the residues involved by comparing the ^{15}N-HSQC spectra of the protein before and after addition of substrate (Figure S3). The ^{15}N-HSQC spectrum shows the cross-peaks of the amide nitrogens and amide hydrogens and is often referred to as the protein's "fingerprint" spectrum. Upon substrate binding, the environment around the nuclei that interact changes and, as a result, the corresponding cross-peak in ^{15}N-HSQC will change. The residues with the highest changes in chemical shift perturbation often belong to the binding site. The biggest differences observed in chemical shifts belong to the side chain of Trp465 ($H^{\varepsilon 1}/N^{\varepsilon 1}$) and Asn466 ($H^{\delta 1}/N^{\delta 1}$ and $H^{\delta 2}/N^{\delta 2}$), corresponding to the interaction surface of the protein. Both have previously been described as most perturbed upon titration with $(GlcNAc)_3$.[13] An overlay of ^{15}N-HSQC for the side chain of Trp465 and Asn466 for CBM14 interacting with $(GlcNAc)_3$ and β-chitin is given by Figure 2 (the diagram comparing all residues is given in Figure S3). The chemical shift perturbation for CBM14 interacting with 6 mg β-chitin is not included as the signals in the ^{15}N-HSQC were broadened beyond detection. As the chemical shift perturbation is more pronounced for β-chitin, it could indicate a stronger binding affinity compared to the soluble $(GlcNAc)_3$.

Another residue that shows a chemical shift perturbation is Thr464. Mutational studies have been done on this threonine and showed medium impact on binding activity for Thr464, which could indicate that this residue could be one of the key polar residues that are directly involved in binding.[13] Furthermore, Cys450 and Cys463 also show a minor change in chemical shift. These cysteins create a disulfide bridge linking the two β-sheets together.

To allow us to obtain detailed information about the bound sugar, we performed T_{1rho} NMR spectroscopy on the CBM14-$(GlcNAc)_3$ system using different protein:ligand concentrations. The resulting one-dimensional (1D) ^{1}H NMR spectra are given in Figure S4. Compared to the reference spectrum, the T_{1rho} experiment will display a reduction in signal intensity if the protein and substrate are bound because the protein's relaxation will be observed on the substrate. We observe indications of substrate binding by getting a reduction in signal intensity for the methyl groups, H1, H2−H6 for $(GlcNAc)_3$. It is evident that CBM14 interacts with $(GlcNAc)_3$ and the nonreducing end of the trimer seems to be preferred (Figure S4). By knowing the binding site (Trp465 and Asn466) in CBM14, we were able to use a docking algorithm (HADDOCK, high-ambiguity driven docking). This showed that the lowest-energy cluster of CBM14 and $(GlcNAc)_3$ coincide with the affected chemical shifts in the T_{1rho} experiments (Figure S4). We also tried to probe the interaction using a water LOGSY[21,22] experiment, but due to the Hβ of the reducing end of $(GlcNAc)_3$ being too close to the frequency for the saturation of the water signal, the spectrum was inconclusive. To support the indicated interactions in the T_{1rho} experiment, we also did a saturation transfer difference (STD)[23,24] experiments varying the protein:ligand concentrations, temperature, saturation times, and on-resonances. However, no detailed information could be extracted from these spectra.

Leu454Ala Mutant. Looking from a structural point of view, this leucine is positioned close to the binding site (Trp465 and Asn466) by β-sheet 2 (β4 and β5). According to a multiple sequence alignment done using Clustal Omega (1.2.4) given by Figure 3, we observe that this particular leucine is conserved in tachycitin, *Pf*Avr4 and *Cf*Avr4. These

DOI: 10.1021/acsomega.9b03043
ACS Omega 2019, 4, 21975−21984

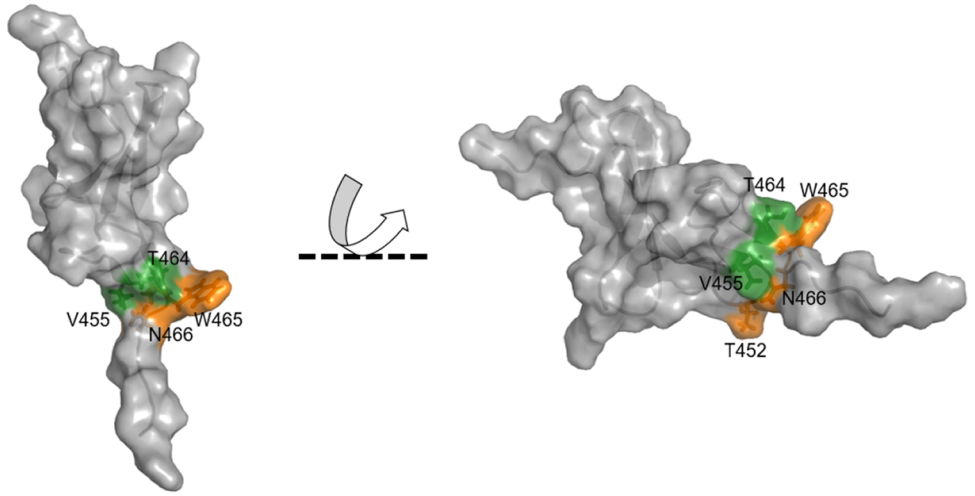

Figure 4. Surface representation of CBM14 showing the residues affected by mutation of Leu454 - > Ala454. The changes are divided into two groups: $\Delta\delta$ 0.2−0.4 ppm (orange): Thr452, side chains of Trp465 and Asn466 and $\Delta\delta$ 0.4−0.8 ppm (green): Val455 and Thr464.

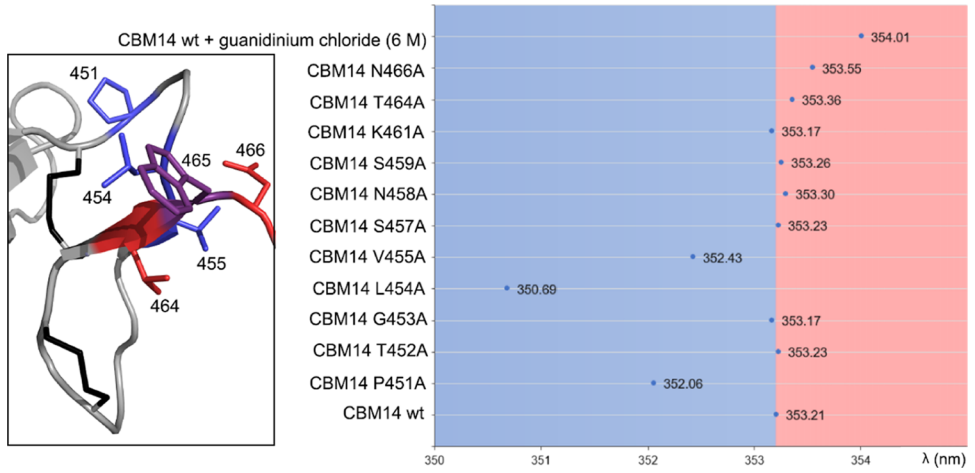

Figure 5. Representation of λ_{max} values of native CBM14 wt, its alanine mutants, and its partially denatured form. The blue and red shifts are represented at the left part (blue) and right part (red) of the diagram. The center of the diagram is aligned to the λ_{max} of CBM14 wt. A structural representation of the residues showing a significant shift are given to the left of the diagram. The residues inducing a blue shift after alanine substitution are colored in blue (Pro451Ala, Leu454Ala, and Val455Ala), and substituted residues inducing a red shift are colored in red (Thr464Ala and Asn466Ala). Disulfide bonds are colored in black and Trp465 in purple.

proteins also have an aromatic residue (tryptophan or tyrosine) in the same position as CBM14's Trp465.

To obtain insight into the differences between CBM14 wild type and CBM14 Leu454Ala mutant, we produced a ^{15}N-labeled mutant and recorded a ^{15}N-HSQC spectrum. The differences in chemical shift compared to the wild type are showed in Figure 4. With a threshold of $\Delta\delta$ 0.2 ppm, five residues showed a significant change in chemical shift. Divided into two groups: $\Delta\delta$ 0.2−0.4 ppm (Thr452, $H^{\varepsilon 1}/N^{\varepsilon 1}$ Trp465 and $H^{\delta 1}/N^{\delta 1}$ and $H^{\delta 2}/N^{\delta 2}$ Asn466) and $\Delta\delta$ 0.4−0.8 ppm (Val455 and Thr464). This mutant has previously been investigated using far-UV CD spectra and β-lactamase enzymatic activity assays,[13] where the conclusion was that CBM14-Leu454Ala demonstrated a reduced chitin-binding affinity compared to the wild type. To investigate this interaction further, we recorded a ^{15}N-HSQC spectrum after addition of $(GlcNAc)_3$. This addition had no effect on the chemical shifts. The interaction was also probed by adding β-chitin, with the same result.

Fluorescence Spectroscopy. Taking advantage of the fact that CBM14 only has one tryptophan (Trp465), we monitored the structural impact of alanine substitutions on key binding residues using fluorescence spectroscopy. The maximum emission wavelength (λ_{max}) provides a measure of the protein's water exposure. The resulting λ_{max} for native CBM14 wild type (wt), denatured (6 M guanidinium chloride), and its mutants are given in Figure 5.

The λ_{max} of the native CBM14 is 353.21 nm, which is explained by the high exposure of Trp465 to the aqueous solvent. Most of the mutants have a similar λ_{max} compared to the native form of CBM14, indicating that an alanine substitution does not modify significantly the direct environment of the Trp465.

A significant blue shift is observed for CBM14-Leu454Ala and to a lesser extent for CBM14-Val455Ala. Both residues are located behind Trp465. A slight blue shift is also observed for CBM14-Pro451A, which can be explained by its position behind the Leu454 and/or its implication in the loop formation (Pro451, Thr452, Gly453, and Leu454). A slight

DOI: 10.1021/acsomega.9b03043
ACS Omega 2019, 4, 21975−21984

red shift is observed for CBM14-Thr464Ala and CBM14-Asn466Ala. This suggests that Trp465 is more exposed to the aqueous solvent in the mutant compared to the wild type due to the smaller side chain of alanine. The highest λ_{max} (354.01 nm) is obtained for the partially denatured sample of CBM14 in 6 M guanidinium chloride.

DISCUSSION

Here, we have focused on the solution structure of CBM14 solved by NMR and how this protein interacts with $(GlcNAc)_3$ and β-chitin. This has led to information about structural elements of this CBM that are vital for its binding affinity. Of particular interest is Leu454, which is important for orienting the main binding residue Trp465 correctly. Both residues, as well as the two aromatic residues creating the hydrophobic core are conserved in other CBM14s, indicating that these residues create a preorganized binding site for the substrate.

Use of NOESY experiments enables observation of a cross-peak between two hydrogen atoms if they are separated by a distance up to 5 Å.[25] This gives rise to a direct determination of the secondary structure of the protein and therefore differences in the residues involved in the β-strands for the X-ray and NMR structures. Together with the three disulfide bridges, the β-sheets maintain the functional conformation of the CBM. Furthermore, the NOESY experiments show NOEs between Phe437 and Phe456. Phe437 is conserved in Der p 23 and tachycitin, but is replaced by a tyrosine in *Cf*Avr4, *Pf*Avr4, and Blo t 12, whereas Phe456 is conserved in Blo t 12, replaced by tyrosine in tachycitin and tryptophan in the three other proteins. These hydrophobic residues that are part of β2 and β4 are commonly found at these positions (except for Blo t 12 where they are part of β4 and β6) and presumably help linking the β-sheets together. This suggests that the two aromatic residues are creating a hydrophobic core that helps stabilize the structure. Altogether, these aspects give rise to the hevein-like fold characteristic for CBM14.

Another trait in CBM14, as with most other CBMs, is that it relies on aromatic residues (often tryptophans) for substrate binding.[3] This CBM14 contains a single tryptophan (Trp465) located on the protein surface in the C-terminus and makes up the binding site for chitin together with Asn466.[13] The tryptophan plays a second role for this CBM by being part of β5 (residues: Cys463-Thr464-Trp465) that is connected to the N-terminal by a disulfide bridge (Cys450-Cys463) and a loop. In this loop region is Leu454 that, together with Val455, was shown to be involved in a hydrophobic pocket important for chitin binding.[13] It is likely that Val455, which is included in the same β-sheet as Phe456 (β4), and displays NOEs to Thr464 (in β5), also assists in the structural integrity of this CBM. This valine is not conserved in other CBM14s and might not play a significant role in the stabilization of the structure, but its neighbor, Leu454, is conserved in the CBM14s that contain an aromatic residue in the same position as our Trp465 (Figure 3).

By looking at the chemical shift perturbation in the ^{15}N-HSQC between the mutant Leu454Ala and wild type, both Val455 and Thr464 display significant changes in chemical shifts. This and the fact that we do not observe any binding activity to either $(GlcNAc)_3$ or β-chitin suggest a disrupted conformation of the CBM and therefore an altered exposure of Trp465 on the protein surface. The importance of Leu454 for the correct positioning of Trp465 is strengthened by the fluorescence spectroscopy data. A significant blue shift is observed for the Leu454Ala mutant, indicating that the tryptophan is less exposed to the surface. When substituted into alanine, the steric hindrance around Trp465 is reduced and leaves more space for this residue to be more buried into the structure of the hevein-like fold. We also observe a smaller blue shift for Val455Ala and Pro451Ala that supports this theory due to their position (right behind Trp465 and in the loop formation, respectively) in this CBM. This indicates that CBM14 could have a preorganized binding site, which means that the role of the hevein-like fold is to keep the tryptophan correctly oriented for efficient substrate binding.

CBM14 is classified as a type C CBM,[3] and it is therefore able to bind short-chain oligosaccharides as also shown by Crasson and co-workers.[13] Out of the tested oligosaccharides, they found that CBM14 had the highest affinity toward $(GlcNAc)_3$. Additionally, this CBM has previously shown a strong affinity for α-chitin,[26] which complements our findings of its ability to bind β-chitin. However, the ability to bind crystalline substrate is a feature that is characteristic of type A CBMs that exhibit a platform-like binding site able to accommodate a crystalline substrate.[3] Interestingly, a comparison of the substrates $(GlcNAc)_3$ and β-chitin shows that the same residues in CBM14 are affected upon substrate binding.

The importance of the polar residues below Trp465, which participate in hydrogen bonding with the polar groups of the polysaccharide, for substrate interaction is supported by the observed change in chemical shift for Thr464. We also observe a minor change in chemical shift for Cys450 and Cys463 (disulfide bridge). Even though these amino acids are not located directly below the binding site, the disulfide bridge they create is pivotal for keeping the structural integrity of the protein intact for binding.

Studies of CBM14's ability to bind chito-oligosaccharides have shown that CBM14 have the best affinity for $(GlcNAc)_3$ (K_d = 9.9 ± 0.8 mM).[13] Our investigation using ITC demonstrated a dissociation constant in the same range with a measured K_d of 3.1 ± 0.2 mM. These K_d's indicate a weak binding affinity to $(GlcNAc)_3$. By comparing the ^{15}N-HSQC of the side chains of Trp465 and Asn466 of CBM14 when it interacts with $(GlcNAc)_3$ or β-chitin (Figure 2), we observe an increase in chemical shift perturbation for the latter. This indicates that CBM14 has a stronger binding affinity toward crystalline substrate compared to the previously observed soluble oligosaccharides.[13]

The relatively weak $(GlcNAc)_3$ binding to CBM14 enabled investigation using T_{1rho} experiments. In Figure S4, we observe a decrease in signal intensity for the methyl groups, H1, and H2−H6 for $(GlcNAc)_3$ in the T_{1rho} experiment, all indicating binding. Ideally, the T_{1rho} spectra could indicate a difference in the trimer's orientation upon binding with CBM14 by giving differences in intensity for the sugar signals. From the experiments shown in Figure S4, we see that the nonreducing end seems to be preferred. This was further tested by using the restraints from the chemical shift perturbation, where Trp465 and Asn466 compose the binding site of CBM14 and a model of the trimer as input in a HADDOCK algorithm. The best model generated supports the observations from the T_{1rho} experiments and suggests a CH−π interaction between the second sugar ring and the side chain of Trp465 (Figure S5).

Even though weak interactions are favored in saturation transfer-based experiments like STD-NMR, detailed information about the $(GlcNAc)_3$ interaction with CBM14 could not be acquired due to spillover from the saturation of the methyl

DOI: 10.1021/acsomega.9b03043
ACS Omega 2019, 4, 21975−21984

region of the protein to the methyl groups of $(GlcNAc)_3$. We have also tried to quantify the binding kinetics (on/off rate) using stopped-flow spectrophotometry, but the reaction was too fast for obtaining kinetic details.

It has previously been suggested[11] that this CBM14 functions as a guiding system for its catalytic domain. Having a CBM help concentrate enzymes onto their substrate is a trait that can be found in other enzyme−CBM systems.[27−30] This can explain the weak binding affinity showed by this CBM as well as its fast on/off rate. A relatively weak binding and an innate fast on/off rate would be beneficial for CBM action. CBMs cannot disrupt the crystalline surface and by this alter the binding interactions resulting in a decreased binding affinity as observed for, e.g., GHs. Here, productive binding yielding hydrolysis reduces the number of binding interactions and greatly weakens the affinity.[31−33]

MATERIALS AND METHODS

Protein Production and Purification. ^{13}C, ^{15}N, and ^{15}N CBM14 samples were expressed in *Escherichia coli* BL21 (DE3) cells. Precultures were grown in Lysogeny broth (LB) medium (10 g/L tryptone, 5 g/L yeast extract, and 5 g/L NaCl) supplemented with 50 μL of kanamycin (50 mg/mL) in a shaking incubator at 30 °C, 225 rpm overnight. Four flasks with 500 mL of LB media and 500 μL of kanamycin (50 mg/mL) in each were inoculated with 1% (v/v) of the overnight culture and grown in a shaking incubator at 30 °C, 225 rpm to $OD_{600} \approx 0.9$ before cooled on ice for 10 min. The cultures were centrifuged (Sorvall) at 4 °C, 6150*g*, for 10 min, and the cells were resuspended on ice in 450 mL of M9 media (6 g/L Na_2HPO_4, 3 g/L KH_2PO_4, 0.5 g/L NaCl) supplemented with 500 μL of kanamycin (50 mg/mL), 1.0 g of $(^{15}NH_4)_2SO_4$, 3 g of glucose (^{15}N label)/2 g of 98% $^{13}C_6$-D-glucose (^{13}C, ^{15}N label) in 10 mL of Milli-Q water, 50 mL of Spectra 9 (Cambridge Isotope Laboratories, Tewksbuty, MA), 5 mL of Gibco MEM Vitamin Solution (100×), 1 mL of 1 M $MgSO_4$, and 5−10 mL of trace-metal solution (0.1 g/L $ZnSO_4$, 0.8 g/L $MnSO_4$, 0.5 g/L $FeSO_4$, 0.1 g/L $CuSO_4$, 1 g/L $CaCl_2$).

After media change, the expression was induced with isopropyl-1-thio-β-D-galactopyranoside to a final concentration of 1 mM and incubated at 16 °C, 225 rpm, for 20 h. The cells were harvested by centrifugation (Sorvall) at 4 °C, 5000*g*, 10 min. Resuspension of the pellet was done in 40 mL of TES buffer at pH 8.0 (3.63 g/L TRIS, 1.86 g/L ethylenediaminetetraacetic acid, 200 g/L sucrose) together with 1/2 tablet cOmplete ULTRA protease inhibitor (Roche) before proceeding with centrifugation (Sorvall) at 4 °C, 6150*g*, 20 min. After removal of supernatant, the cells were incubated at room temperature for 10 min and then resuspended in 30 mL of MQ and 1/2 tablet cOmplete ULTRA protease inhibitor (Roche). The suspension was added to 125 μL of 1 M $MgSO_4$ before the final centrifugation (Sorvall) at 13 000*g*, 45 min. The supernatant was filtered through a 0.2 μm Sterile-flip filter unit (Nalgene).

Purification of the protein was done on an ÄKTA FPLC instrument equipped with an anion exchange column (1 mL HisTrap, FF, GE Healthcare Life Sciences) with a flow rate of 1 mL/min after the following measures: The column was equilibrated with five column volumes (CV) of equilibration buffer at pH 8.0 (300 mM KCl, 50 mM KH_2PO_4, 5 mM imidazole). The periplasmic extract was loaded onto the column and unbound protein was removed by 6 CV equilibration buffer followed by 6 CV washing buffer at pH 8.0 (300 mM KCl, 50 mM KH_2PO_4, 10 mM imidazole). The protein was eluted with elution buffer at pH 8.0 (300 mM KCl, 50 mM KH_2PO_4, 250 mM imidazole). Sodium dodecyl sulfate-polyacrylamide gel electrophoresis was used to confirm the separation and purity of the mature CBM14.

The fractions were then combined and dialyzed (MWCO 6−8 kDa) with desalting buffer pH 8.0 (20 mM TRIS, 50 mM NaCl) (2 h + overnight) and thrombin digestion buffer pH 8.0 (20 mM TRIS, 50 mM NaCl, 5 mM $CaCl_2$) (2 h + 2 h).

The isolated CBM14 was released from the carrier protein by thrombin cleavage (2−3 U thrombin pr mg protein) at room temperature, 3−4 rpm for 2 h before adding cOmplete ULTRA protease inhibitor (Roche).

An ÄKTA FPLC instrument equipped with a size-exclusion chromatography (SEC) column (HiLoad Superdex 75 pg) was equilibrated with SEC-buffer at pH 7.5 (20 mM TRIS, 50 mM NaCl) for 20 h. The flow rate was 1 mL/min. Fractions containing CBM14 were concentrated and buffer-exchanged into the NMR buffer (50 mM sodium phosphate, pH 5.5 or pH 7.0) for interaction studies. Samples for NMR were made with CBM14 in NMR buffer with D_2O added to a final ratio of 90% H_2O/10% D_2O) by centrifugation using Vivaspin 6 protein spin concentrators (MWCO 3 kDa, Sartorius) at 10 °C, 7000*g*.

Generation of Mutants of CBM14. Alanine mutants of CBM14 were generated as previously described by Crasson and co-workers.[13] The ^{15}N CBM14 Leu454Ala mutant was produced and purified as described above.

NMR Spectroscopy. All CBM14 NMR samples were prepared in 50 mM sodium phosphate buffer and 10% D_2O, pH 5.5 or pH 7.0 (interaction studies).

The spectra were recorded at 25 °C on a Bruker Ascend 800 MHz spectrometer Avance III HD (Bruker Biospin) equipped with a 5 mm Z-gradient CP-TCI (H/C/N) cryoprobe at the NV-NMR-Centre/Norwegian NMR Platform at NTNU Norwegian University of Science and Technology, Trondheim, Norway. ^1H shifts were referenced internally to the water signal, while ^{13}C and ^{15}N chemical shifts were referenced indirectly to HDO based on the absolute frequency ratios.[34] Backbone and side-chain assignments of CBM14 were achieved using ^{15}N-HSQC, ^{13}C-HSQC, HNCA, HN(CO)CA, HNCO, HN(CA)CO, HNCACB, HN(CO)CACB, H(C)CH-TOCSY, H(CCCO)NH, ^{15}N-edited NOESY-HSQC, and ^{13}C-edited aliphatic NOESY-HSQC. The NMR data were recorded and processed with TopSpin version 3.5, and the data were analyzed with CARA version 1.5.[35] Backbone torsion angles were predicted using TALOS-N (https://spin.niddk.nih.gov/bax/software/TALOS-N/)[36] and chemical shits of N, H^N, C^α, C^β, H^α, H^β, and C′.

Structure Elucidation. NOE distance restraints were obtained using ^{15}N-edited NOESY-HSQC and ^{13}C-edited aliphatic NOESY-HSQC. Backbone torsion angles predicted by TALOS-N[36] were used as constraints for structure calculation, as were the three disulfide bridges Cys420-Cys440, Cys450-Cys463, and Cys460-Cys462. This information enabled structure calculation using CYANA 3.98[37,38] by generating 100 structures that were optimized using 10 000 steps of simulated annealing. Using YASARA[39] with a YASARA force field,[40] energy minimization was done on the 20 conformers with lowest CYANA target function values (Table S1).

Substrate Binding. The interaction between CBM14 and β-chitin (Mahtani Chitosan, Veraval, Gujarat, India, milled and

DOI: 10.1021/acsomega.9b03043
ACS Omega 2019, 4, 21975−21984

sieved to a particle size of ca. 0.5 mm) was investigated using NMR spectroscopy. A ^{15}N-HSQC spectrum of 90 μM CBM14 in 50 mM sodium phosphate buffer and 10% D_2O, pH 7.0, was recorded at 25 °C as reference. New ^{15}N-HSQC spectra were recorded after addition of β-chitin (1, 2, and 6 mg). The change in chemical shift $\Delta\delta$ (in ppm) was calculated using the following formula: $\Delta\delta = ((\Delta\delta_H)^2 + (\Delta\delta_N/5)^2)^{1/2}$,[41] where $\Delta\delta_H$ and $\Delta\delta_N$ are the change in chemical shift for the amide proton and amide nitrogen (ppm), respectively. The interaction between CBM14 and $(GlcNAc)_3$ was done as described by Crasson and co-workers.[13]

In addition, interaction studies were carried out with the mutant, 90 μM ^{15}N CBM14 Leu454Ala with two substrates: $(GlcNAc)_3$ (Seikagaku Corporation, Tokyo, Japan) (12 mM) and β-chitin (6 mg).

The interaction between CBM14 and $(GlcNAc)_3$ was studied by saturation transfer difference (STD)-NMR using the following pulse programs: water LOGSY,[21,22] STD,[23,24] and T_{1rho} (a spinlock element to measure the T_{1rho} was incorporated in a normal proton experiment with excitation sculping for water suppression). The water LOGSY was performed at 25 °C in a 3 mm NMR tube containing 26 μM CBM14 and 400 μM $(GlcNAc)_3$ (protein:ligand ratio, 1:15) in 50 mM sodium phosphate buffer and 10% D_2O, pH 7.0. For the STD and T_{1rho} experiments, four different protein:ligand concentrations (1:100: 3 μM CBM14 and 300 μM $(GlcNAc)_3$; 1:50: 5 μM CBM14 and 260 μM $(GlcNAc)_3$; 3:50: 15 μM CBM14 and 260 μM $(GlcNAc)_3$; and 1:15: 26 μM CBM14 and 400 μM $(GlcNAc)_3$) were tested at 25 °C. The STD experiments were also done at 15 °C and tested at different saturation times (0.40, 0.50, 0.75, 0.80, 1.20, 1.60, 2.00, 2.50, 3.00, 4.00, 5.00 s). The on-resonance frequency was set in the aliphatic region (0.28, 0.37, and 0.82 ppm), and the off-resonance frequency at −30 ppm.

Docking. High-ambiguity driven biomolecular docking (HADDOCK) was used to get further insight into the interaction between CBM14 and $(GlcNAc)_3$. The docking was carried out using the Easy interface of HADDOCK 2.2 (https://haddock.science.uu.nl/services/HADDOCK2.2/haddockserver-easy.html).[42] The PDB file containing the NMR structure of CBM14 and a model of $(GlcNAc)_3$ was uploaded after being generated by GLYCAM Carbohydrate builder (glycam.org). Active residues were Trp465 and Asn466, and passive residues were determined automatically by HADDOCK as those within a radius of 6.5 Å.

Isothermal Titration Calorimetry. Isothermal titration calorimetry (ITC) was performed using the VP-ITC system from Microcal, Inc. (Northampton, MA).[19] Buffered solutions of 20 mM TRIS and 50 mM NaCl, pH 7.5, were thoroughly degassed prior to experiments to avoid air bubbles in the calorimeter. An enzyme concentration of 45 μM was used in the reaction cell with a volume of 1.42 mL and 12 mM $(GlcNAc)_3$ was used in the ITC syringe. Aliquots of 8 μL were injected into the reaction cell at 200 s intervals. The stirring speed was set to be 260 rpm. The titrations were performed at t = 15 °C and were completed after 40 injections. ITC data were collected automatically using the Microcal Origin version 7.0 software associated with the VP-ITC system. Prior to further analysis, all data were corrected for heat of dilution by subtracting the heat produced by titrating 12 mM $(GlcNAc)_3$ into plain buffer. The fitting of data took place by utilizing a nonlinear least-squares algorithm using a single-site binding model employed by the Origin software, yielding the equilibrium binding association constant (K_a) and the enthalpy change ($\Delta H_r°$). The stoichiometry (n) was set to be 1 based on the knowledge from the NMR experiments. Errors in K_a and $\Delta H_r°$ were obtained as standard deviations from four individual experiments. K_d, $\Delta G_r°$, $\Delta S_r°$, and $-T\Delta S_r°$ were calculated from eq 2, and errors in these parameters were obtained from propagation of error.

Fluorescence Spectroscopy. The partially denatured CBM14 was prepared by incubating the protein in 6 M guanidinium chloride during 24 h at 4 °C. Proteins were used at 16 μM in 8 mM phosphate (Na_2HPO_4/NaH_2PO_4) and 16 mM NaCl buffer, pH 7.5. A Varian Cary Eclipse fluorimeter was used with the software Scan (version 1.1) to analyze the intrinsic fluorescence of all of the samples. The device was set up as follows: Excitation wavelength: 295 nm, measured wavelengths: 300−400 nm, excitation fast filter: 2.5 nm, emission fast filter: 5.0 nm, temperature: 25 °C, with 20 scans for each sample.

■ ASSOCIATED CONTENT

Supporting Information

The Supporting Information is available free of charge at https://pubs.acs.org/doi/10.1021/acsomega.9b03043.

^{1}H,^{15}N-HSQC spectrum of ^{13}C, ^{15}N-labeled CBM14 (0.1 mM) (Figure S1); restraints and structural statistics for the 20 best conformers of CBM14 (PDB ID: 6SO0) (Table S1); residues involved in β-strands from the crystal (PDB ID: 5HBF) and NMR structure of CBM14 (Table S2); binding isotherm with theoretical fits obtained for the titration of $(GlcNAc)_3$ against CBM14 (Figure S2); chemical shift perturbation for CBM14 interacting with either β-chitin or $(GlcNAc)_3$ (Figure S3); T_{1rho} 1D ^{1}H NMR spectra of CBM14 and $(GlcNAc)_3$ (Figure S4); and proposed model of the interaction between CBM14 and $(GlcNAc)_3$ using HADDOCK (Figure S5) (PDF)

■ AUTHOR INFORMATION

Corresponding Author

*E-mail: finn.l.aachmann@ntnu.no. Phone: +47 735 93 317.

ORCID

Eva Madland: 0000-0001-7124-2638

Morten Sørlie: 0000-0001-7259-6710

Finn L. Aachmann: 0000-0003-1613-4663

Notes

The authors declare no competing financial interest.

■ ACKNOWLEDGMENTS

This work was financed by SO-funds from NTNU, Norwegian University of Science and Technology, and by the Norwegian NMR Platform (supported by the Norwegian Research Council, grant number 226244). The authors thank Gerd Inger Sætrom for excellent technical assistance and Dr. Gaston Courtade for helping with the YASARA energy minimization and providing the solid β-chitin granular.

■ REFERENCES

(1) Aboitiz, N.; Vila-Perello, M.; Groves, P.; Asensio, J. L.; Andreu, D.; Canada, F. J.; Jimenez-Barbero, J. NMR and modeling studies of protein-carbohydrate interactions: synthesis, three-dimensional structure, and recognition properties of a minimum hevein domain with

DOI: 10.1021/acsomega.9b03043
ACS Omega 2019, 4, 21975−21984

binding affinity for chitooligosaccharides. *ChemBioChem* **2004**, *5*, 1245−1255.
(2) Guillen, D.; Sanchez, S.; Rodriguez-Sanoja, R. Carbohydrate-binding domains: multiplicity of biological roles. *Appl. Microbiol. Biotechnol.* **2010**, *85*, 1241−1249.
(3) Boraston, A. B.; Bolam, D. N.; Gilbert, H. J.; Davies, G. J. Carbohydrate-binding modules: fine-tuning polysaccharide recognition. *Biochem. J.* **2004**, *382*, 769−781.
(4) Rinaudo, M. Main properties and current applications of some polysaccharides as biomaterials. *Polym. Int.* **2008**, *57*, 397−430.
(5) Lee, C. G.; Da Silva, C. A.; Lee, J. Y.; Hartl, D.; Elias, J. A. Chitin regulation of immune responses: an old molecule with new roles. *Curr. Opin. Immunol.* **2008**, *20*, 684−689.
(6) Zelensky, A. N.; Gready, J. E. The C-type lectin-like domain superfamily. *FEBS J.* **2005**, *272*, 6179−6217.
(7) Hussain, M.; Wilson, J. B. New paralogues and revised time line in the expansion of the vertebrate GH18 family. *J. Mol. Evol.* **2013**, *76*, 240−260.
(8) Boot, R. G.; Blommaart, E. F.; Swart, E.; Ghauharali-van der Vlugt, K.; Bijl, N.; Moe, C.; Place, A.; Aerts, J. M. Identification of a novel acidic mammalian chitinase distinct from chitotriosidase. *J. Biol. Chem.* **2001**, *276*, 6770−6778.
(9) Renkema, G. H.; Boot, R. G.; Strijland, A.; Donker-Koopman, W. E.; Berg, M.; Muijsers, A. O.; Aerts, J. M. Synthesis, sorting, and processing into distinct isoforms of human macrophage chitotriosidase. *Eur. J. Biochem.* **1997**, *244*, 279−285.
(10) Lombard, V.; Golaconda, H. R.; Drula, E.; Coutinho, P. M.; Henrissat, B. The carbohydrate-active enzymes database (CAZy) in 2013. *Nucleic Acids Res.* **2014**, *42*, D490−D495.
(11) Fadel, F.; Zhao, Y.; Cousido-Siah, A.; Ruiz, F. X.; Mitschler, A.; Podjarny, A. X-ray crystal structure of the full length human chitotriosidase (CHIT1) reveals features of its chitin binding domain. *PLoS One* **2016**, *11*, No. e0154190.
(12) Tjoelker, L. W.; Gosting, L.; Frey, S.; Hunter, C. L.; Trong, H. L.; Steiner, B.; Brammer, H.; Gray, P. W. Structural and functional definition of the human chitinase chitin-binding domain. *J. Biol. Chem.* **2000**, *275*, 514−520.
(13) Crasson, O.; Courtade, G.; Leonard, R. R.; Aachmann, F. L.; Legrand, F.; Parente, R.; Baurain, D.; Galleni, M.; Sorlie, M.; Vandevenne, M. Human chitotriosidase: catalytic domain or carbohydrate binding module, who's leading HCHT's biological function. *Sci. Rep.* **2017**, *7*, No. 2768.
(14) Stockinger, L. W.; Eide, K. B.; Dybvik, A. I.; Sletta, H.; Varum, K. M.; Eijsink, V. G.; Tondervik, A.; Sorlie, M. The effect of the carbohydrate binding module on substrate degradation by the human chitotriosidase. *Biochim. Biophys. Acta* **2015**, *1854*, 1494−1501.
(15) Suetake, T.; Tsuda, S.; Kawabata, S.; Miura, K.; Iwanaga, S.; Hikichi, K.; Nitta, K.; Kawano, K. Chitin-binding proteins in invertebrates and plants comprise a common chitin-binding structural motif. *J. Biol. Chem.* **2000**, *275*, 17929−17932.
(16) Mueller, G. A.; Randall, T. A.; Glesner, J.; Pedersen, L. C.; Perera, L.; Edwards, L. L.; DeRose, E. F.; Chapman, M. D.; London, R. E.; Pomes, A. Serological, genomic and structural analyses of the major mite allergen Der p 23. *Clin. Exp. Allergy* **2016**, *46*, 365−376.
(17) Kohler, A. C.; Chen, L. H.; Hurlburt, N.; Salvucci, A.; Schwessinger, B.; Fisher, A. J.; Stergiopoulos, I. Structural analysis of an Avr4 effector ortholog offers insight into chitin binding and recognition by the Cf-4 receptor. *Plant Cell* **2016**, *28*, 1945−1965.
(18) Hurlburt, N. K.; Chen, L. H.; Stergiopoulos, I.; Fisher, A. J. Structure of the *Cladosporium fulvum* Avr4 effector in complex with (GlcNAc)6 reveals the ligand-binding mechanism and uncouples its intrinsic function from recognition by the Cf-4 resistance protein. *PLoS Pathog.* **2018**, *14*, No. e1007263.
(19) Wiseman, T.; Williston, S.; Brandts, J. F.; Lin, L. N. Rapid measurement of binding constants and heats of binding using a new titration calorimeter. *Anal. Biochem.* **1989**, *179*, 131−137.
(20) Turnbull, W. B.; Daranas, A. H. On the value of c: Can low affinity systems be studied by isothermal titration calorimetry? *J. Am. Chem. Soc.* **2003**, *125*, 14859−14866.
(21) Dalvit, C.; Fogliatto, G.; Stewart, A.; Veronesi, M.; Stockman, B. WaterLOGSY as a method for primary NMR screening: Practical aspects and range of applicability. *J. Biomol. NMR* **2001**, *21*, 349−359.
(22) Dalvit, C. Efficient multiple-solvent suppression for the study of the interactions of organic solvents with biomolecules. *J. Biomol. NMR* **1998**, *11*, 437−444.
(23) Mayer, M.; Meyer, B. Characterization of ligand binding by saturation transfer difference NMR spectroscopy. *Angew. Chem., Int. Ed.* **1999**, *38*, 1784−1788.
(24) Mayer, M.; Meyer, B. Group epitope mapping by saturation transfer difference NMR to identify segments of a ligand in direct contact with a protein receptor. *J. Am. Chem. Soc.* **2001**, *123*, 6108−6117.
(25) Braun, W.; Bösch, C.; Brown, L. R.; Go, N.; Wütrich, K. Combined use of proton-proton Overhauser enhancements and a distance geometry algorithm for determination of polypeptide conformations. *Biochim. Biophys. Acta* **1981**, *667*, 377−396.
(26) Vandevenne, M.; Campisi, V.; Freichels, A.; Gillard, C.; Gaspard, G.; Frere, J. M.; Galleni, M.; Filee, P. Comparative functional analysis of the human macrophage chitotriosidase. *Protein Sci.* **2011**, *20*, 1451−1463.
(27) Hall, J.; Black, G. W.; Ferreira, L. M.; Millward-Sadler, S. J.; Ali, B. R.; Hazlewood, G. P.; Gilbert, H. J. The non-catalytic cellulose-binding domain of a novel cellulase from *Pseudomonas fluorescens* subsp. cellulosa is important for the efficient hydrolysis og Avicel. *Biochem. J.* **1995**, *309*, 749−756.
(28) Bolam, D. N.; Ciruela, A.; McQueen-Mason, S.; Simpson, P.; Williamson, M. P.; Rixon, J. E.; Boraston, A.; Hazlewood, G. P.; Gilbert, H. J. *Pseudomonas* cellulose-binding domains mediate their effects by increasing enzyme substrate proximity. *Biochem. J.* **1998**, *331*, 775−781.
(29) Herve, C.; Rogowski, A.; Blake, A. W.; Marcus, S. E.; Gilbert, H. J.; Knox, J. P. Carbohydrate-binding modules promote the enzymatic deconstruction of intact plant cell walls by targeting and proximity effects. *Proc. Natl. Acad. Sci. U.S.A.* **2010**, *107*, 15293−15298.
(30) Crouch, L. I.; Labourel, A.; Walton, P. H.; Davies, G. J.; Gilbert, H. J. The contribution of non-catalytic carbohydrate binding modules to the activity of lytic polysaccharide monooxygenases. *J. Biol. Chem.* **2016**, *291*, 7439−7449.
(31) Zolotnitsky, G.; Cogan, U.; Adir, N.; Solomon, V.; Shoham, G.; Shoham, Y. Mapping glycoside hydrolase substrate subsites by isothermal titration calorimetry. *Proc. Natl. Acad. Sci. U.S.A.* **2004**, *31*, 11275−11280.
(32) Norberg, A. L.; Karlsen, V.; Hoell, I. A.; Bakke, I.; Eijsink, V. G.; Sorlie, M. Determination of substrate binding energies in individual subsites of a family 18 chitinase. *FEBS Lett.* **2010**, *584*, 4581−4585.
(33) Kurasin, M.; Kuusk, S.; Kuusk, P.; Sorlie, M.; Valjamae, P. Slow off-rates and strong product binding are required for processivity and efficient degradation of recalcitrant chitin by family 18 chitinases. *J. Biol. Chem.* **2015**, *290*, 29074−29085.
(34) Zhang, H.; Neal, S.; Wishart, D. S. RefDB: A database of uniformly referenced protein chemical shifts. *J. Biomol. NMR* **2003**, *25*, 173−195.
(35) Keller, R. *The Computer Aided Resonance Assignment*; C. Verlag: Goldau, Switzerland, 2004.
(36) Shen, Y.; Bax, A. Protein backbone and sidechain torsion angles predicted from NMR chemical shifts using artificial neural networks. *J. Biomol. NMR* **2013**, *56*, 227−241.
(37) Güntert, P.; Mumenthaler, C.; Wüthrich, K. Torsion angle dynamics for NMR structure calculation with the new program DYANA. *J. Mol. Biol.* **1997**, *273*, 283−298.
(38) Güntert, P. Automated NMR Structure Calculation with CYANA. In *Protein NMR Techniques*; Downing, A. K., Ed.; Humana Press: Totowa, NJ, 2004; pp 353−378.
(39) Krieger, E.; Koraimann, G.; Vriend, G. Increasing the precision of comparative models with YASARA NOVA–a self-parameterizing force field. *Proteins* **2002**, *47*, 393−402.

DOI: 10.1021/acsomega.9b03043
ACS Omega 2019, 4, 21975−21984

(40) Krieger, E.; Joo, K.; Lee, J.; Lee, J.; Raman, S.; Thompson, J.; Tyka, M.; Baker, D.; Karplus, K. Improving physical realism, stereochemistry, and side-chain accuracy in homology modeling: Four approaches that performed well in CAPS8. *Proteins* **2009**, *77*, 114−122.
(41) Mulder, F. A. A.; Schipper, D.; Bott, R.; Boelens, R. Altered flexibility in the substrate-binding site of related native and engineered high-alkaline Bacillus subtilisins. *J. Mol. Biol.* **1999**, *292*, 111−123.
(42) van Zundert, G. C. P.; Rodrigues, J.; Trellet, M.; Schmitz, C.; Kastritis, P. L.; Karaca, E.; Melquiond, A. S. J.; van Dijk, M.; de Vries, S. J.; Bonvin, A. The HADDOCK2.2 Web Server: User-Friendly Integrative Modeling of Biomolecular Complexes. *J. Mol. Biol.* **2016**, *428*, 720−725.

DOI: 10.1021/acsomega.9b03043
ACS Omega 2019, 4, 21975−21984